A precise measurement of 180 GeV muon energy losses in iron

P. Amaral, A. Amorim, K. Anderson, A. Artikov, R. Benetta, S. Berglund, C. Biscarat, O. Blanch, G. Blanchot, A. Bogush, et al.

Eur. Phys. J. C 20, 487–495 (2001)
Digital Object Identifier (DOI) 10.1007/s100520100645

THE EUROPEAN PHYSICAL JOURNAL C

A precise measurement of 180 GeV muon energy losses in iron

The ATLAS TileCal Collaboration

P. Amaral[11], A. Amorim[11], K. Anderson[6], A. Artikov[8], R. Benetta[10], S. Berglund[20], C. Biscarat[7], O. Blanch[3], G. Blanchot[3], A. Bogush[14], C. Bohm[20], V. Boldea[5], O. Borisov[8], M. Bosman[3], C. Bromberg[9], S. Bravo[3], J. Budagov[8], S. Burdin[15], L. Caloba[19], F. Camarena[22], J. Carvalho[12], M. V. Castillo[22], M. Cavalli-Sforza[3], V. Cavasinni[15], A. S. Cerqueira[19], R. Chadelas[7], I. Chirikov-Zorin[8], G. Chlachidze[8,*], M. Cobal[10], F. Cogswell[21], S. Cologna[15], S. Constantinescu[5], D. Costanzo[15], B. Cowan[6], M. Crouau[7], F. Daudon[7], M. David[11], T. Davidek[16], J. Dawson[1], K. De[2], M. Delfino[3], T. Del Prete[15], A. De Santo[15], B. Di Girolamo[15], S. Dita[5], R. Downing[21], M. Engström[20], D. Errede[21], S. Errede[21], F. Fassi[22], A. Fenyuk[18], A. Ferrer[22], V. Flaminio[15], J. Flix[3], R. Garabik[4], I. Gil[22], O. Gildemeister[10], V. Glagolev[8], A. Gomes[11], V. Gonzalez[22], S. González De La Hoz[22], V. Grabski[23], P. Grenier[7], H. Hakopian[23], M. Haney[21], S. Hellman[20], A. Henriques[10], C. Hebrard[7], E. Higon[22], P. Holik[4], S. Holmgren[20], I. Hruska[17], J. Huston[9], K. Jon-And[20], S. Kakurin[8], A. Karyukhin[18], J. Khubua[8,⋆], S. Kopikov[18], P. Krivkova[16], V. Kukhtin[8], Y. Kulchitsky[14,8] M. Kuzmin[14], S. Lami[15], V. Lapin[18], C. Lazzeroni[15], A. Lebedev[8], R. Leitner[16], J. Li[2], Yu. Lomakin[8], O. Lomakina[8], M. Lokajicek[17], J. M. Lopez Amengual[22], A. Maio[11], S. Malyukov[8], F. Marroquin[19], L. Mataix[22], E. Mazzoni[15], F. Merritt[6], R. Miller[9], I. Minashvili[8,⋆], Ll. Miralles[3], G. Montarou[7], S. Nemecek[17], M. Nessi[10], A. Onofre[13], A. Ostankov[3], A. Pacheco[3], D. Pallin[7], D. Pantea[5,8] R. Paoletti[15], I.C. Park[3], J. Pilcher[6], J. Pinhão[12], L. Price[1], J. Proudfoot[1], O. Pukhov[8], G. Reinmuth[7], G. Renzoni[13], R. Richards[9], C. Roda[13], J. Roldan[22], J. B. Romance[22], V. Romanov[8], P. Rosnet[7], H. Ruiz[3], N. Russakovich[8], E. Sanchis[22], H. Sanders[6], C. Santoni[7], J. Santos[11], L.-P. Says[7], J. M. Seixas[19], B. Selldèn[20], A. Semenov[8], A. Shchelchkov[8], M. Shochet[6], J. Silva[11], V. Simaitis[21], A. Sissakian[8], A. Solodkov[18], O. Solovianov[18], M. Sosebee[2], K. Soustruznik[16], F. Spanó[15], R. Stanek[1], E. Starchenko[18], P. Stavina[4], M. Suk[16], I. Sykora[4], F. Tang[6], P. Tas[16], J. Thaler[21], Z. D. Thome-Filho[19], S. Tokar[4], N. Topilin[8], S. Valkar[16], M. J. Varanda[11], A. Vartapetian[2,23] F. Vazeille[7], I. Vichou[3], V. Vinogradov[8], S. Vorozhtsov[8], A. White[2], H. Wolters[13], N. Yamdagni[20], G. Yarygin[8], C. Yosef[9], A. Zaitsev[18]

[1] Argonne National Laboratory, Argonne, IL, USA
[2] University of Texas at Arlington, Arlington, TX, USA
[3] Institut de Fisica d'Altes Energies, Universitat Autònoma de Barcelona, Barcelona, Spain
[4] Comenius University, Bratislava, Slovakia
[5] Institute of Atomic Physics, Bucharest, Rumania
[6] University of Chicago, Chicago, IL, USA
[7] LPC Clermont–Ferrand, Université Blaise Pascal / CNRS–IN2P3, Clermont–Ferrand, France
[8] JINR, Dubna, Russia
[9] Michigan State University, East Lansing, MI, USA
[10] CERN, Geneva, Switzerland
[11] LIP Lisbon and FCUL Univ. of Lisbon, Portugal
[12] LIP and FCTUC Univ. of Coimbra, Portugal
[13] Univ. Católica Figueira da Foz, Portugal
[14] Institute of Physics, National Academy of Sciences, Minsk, Republic of Belarus
[15] Pisa University and INFN, Pisa, Italy
[16] Charles University in Prague, Prague, Czech Republic
[17] Academy of Sciences of the Czech Republic, Prague, Czech Republic
[18] Institute for High Energy Physics, Protvino, Russia
[19] COPPE/EE/UFRJ, Rio de Janeiro, Brazil
[20] Stockholm University, Stockholm, Sweden
[21] University of Illinois, Urbana–Champaign, IL, USA
[22] IFIC, Centro Mixto Universidad de Valencia-CSIC, 46100 Burjassot, Valencia, Spain
[23] Yerevan Physics Institute, Yerevan, Armenia

Received: 28 December 2000 / Revised version: 14 February 2001 /
Published online: 28 May 2001 –

Abstract. The energy loss spectrum of 180 GeV muons has been measured with the 5.6 m long finely segmented Module 0 of the ATLAS hadron Tile Calorimeter at the CERN SPS. The differential probability $\mathrm{d}P/\mathrm{d}v$ per radiation length of a fractional energy loss $v = \Delta E_\mu/E_\mu$ has been measured in the range $0.025 \leq v \leq 0.97$; it is compared with theoretical predictions for energy losses due to bremsstrahlung, production of electron–positron pairs, and energetic knock-on electrons. The iron elastic form factor correction $\Delta_{Fe}^{el} = 1.63 \pm 0.17_{stat} \pm 0.23_{syst} \pm^{0.20}_{0.14 theor}$ to muon bremsstrahlung in the region of no screening of the nucleus by atomic electrons has been measured for the first time, and is compared with different theoretical predictions.

1 Introduction

The detection and measurement of muons with energies in excess of 100 GeV at the Large Hadron Collider will be important for the investigation of a wide variety of physics processes (intermediate boson decays, jets with heavy flavour tags, etc.). In the ATLAS [1] detector, muons will be measured by tracking chambers within a toroidal air-core magnet after they have crossed more than 100 radiation lengths of material in the electromagnetic and hadronic calorimeters. It is, therefore, important to check precisely the theoretical predictions for muon energy losses in iron or higher Z materials.

Muons undergo the same electromagnetic processes as electrons. However, the relative contributions of the electron–positron pair production, production of knock-on electrons and the bremsstrahlung process for muons and electrons are very different (see Fig. 1). The radiative energy losses of electrons and positrons are well understood and checked against the QED predictions, while a few uncertainties still exist for muons.

A precise knowledge of the muon energy losses is also important for the interpretation of the data taken in current underground and underwater experiments. Recently a variety of new theoretical calculations has been done. The radiative corrections to knock-on electron production and muon bremsstrahlung on atomic electrons recently calculated in [2] increase the probability of muon energy losses. It was pointed out by Tannenbaum [3] that the main uncertainties in the description of bremsstrahlung are due to the different theoretical predictions of the nuclear size correction. This correction is important for muon bremsstrahlung, while for electrons, it is negligible due to its low mass. New calculations of the nuclear size correction have been reported in [4,5]. The contribution of diffractive corrections to muon bremsstrahlung [6] is important for the losses of high energy positively charged muons in light materials.

Energy losses of muons at very high energies, up to 10 TeV, have been measured in cosmic-ray experiments [7–9]. In these experiments muon energies were measured with a magnetic spectrometer, and reasonable agreement between data and calculations was found, but not in the region of very small energy losses [9]. Energy losses of muons up to 300 GeV were measured in various accelerator experiments [10–14]. A reasonable agreement with theory was reported in [10–12]. Preliminary results of 300 GeV muon energy loss measurements in iron (lead) indicated [13] about 7% (10%) higher probability compared to Monte Carlo predictions.

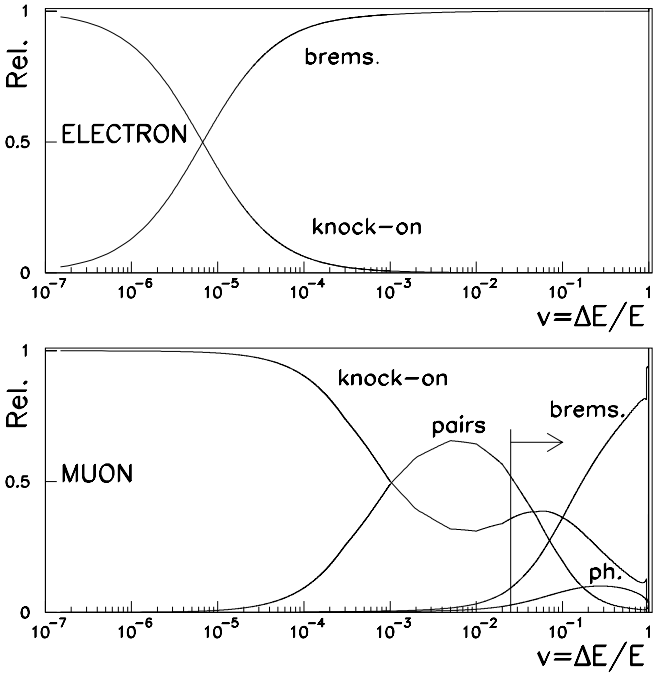

Fig. 1. Relative probabilities of fractional energy losses $v = \Delta E/E$ **per interaction** and per radiation length of iron, for 180 GeV electrons (top plot) and muons (bottom plot), due to different processes. The arrow indicates the region of muon energy losses studied in the present experiment. For muons, the contributions of knock-on electron production (knock-on), electron–positron pair production (pairs), bremsstrahlung (brems.) and photonuclear interactions (ph.) have been calculated according to the formulas given in the text. For electrons, the same formulas have been used, replacing the elctron mass with the muon mass

In an earlier experiment [14] by the authors of this paper, the energy loss spectrum of 150 GeV muons in 1 meter long prototype modules of the ATLAS Tile Calorimeter was studied. The spectrum of muon energy losses was found to be in very good agreement with theoretical predictions, and an indication of a non–zero value of the nuclear size correction to the bremsstrahlung process was found. The main limitation on the precision of the measurement was due to to the systematic uncertainty of the calorimeter energy scale calibration.

In this paper, a measurement performed in 1998 with 180 GeV positive muons incident on a preseries module of the ATLAS Tile Calorimeter (Module 0) is described. In this setup muons traversed 5.6 m of finely segmented iron and scintillators, thereby providing high statistics and high granularity data. Compared to the past study, the

⋆ On leave from HEPI, Tbilisi State Univ., Georgia

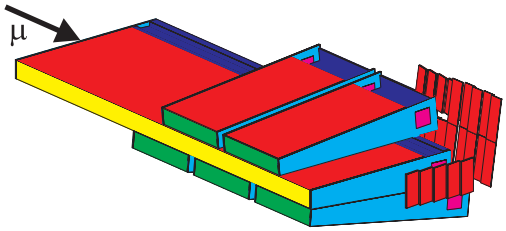

Fig. 2. The experimental setup. The muon beam indicated by the arrow enters in the center of 5.6 m long Module 0 from the left side. At the downstream end, the large calorimeter was surrounded below by three 1-meter long small calorimeters and above by two of them

fiducial region for observing large energy losses is much longer (115.3 radiation lengths, *vs*. 17.6 r.l. in [14]) and contamination from hadrons and muon decays in flight are eliminated using the first 1.5 m of the muon track in the calorimeter.

The results are compared with theoretical predictions. Particular attention is given to muon bremsstrahlung which is the dominant process leading to large energy losses. In this region we clearly observed for the first time the suppression of bremsstrahlung due to the nuclear elastic form factor.

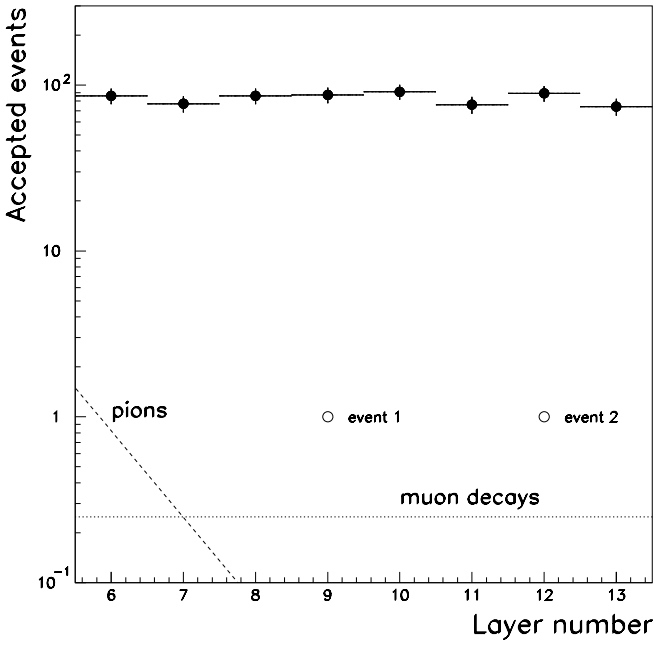

Fig. 3. Data contamination by electrons and pions. Full circles are the positions of maxima of accepted showers with energy greater than 70 GeV. The curves correspond to the expected contamination of the data by pion induced showers and by muon decays in flight. The empty circles indicate the two events compatible with muon decays in flight

2 Experiment and data analysis

The ATLAS Tile Calorimeter is an iron-scintillator sampling calorimeter read out with wavelength-shifting fibres. An important feature of this calorimeter is orientation of the scintillator tiles perpendicular to the colliding beams; a detailed description of the calorimeter concept, the Module 0 and prototypes is given elsewhere [15]. For the purpose of this measurement, the Module 0 and the 1-meter small modules of the calorimeter were placed in the H8 beam of the CERN SPS, and oriented so that particles cross the tiles of Module 0 at perpendicular incidence (Fig. 2). The 5.6 m long Module 0 was surrounded at the downstream end by three small modules on the bottom and two on the top (see Fig. 2). The beam entered in the center of the Module 0.

In this configuration the muon beam traverses periods of alternating slabs of iron (14 mm) and scintillators (3 mm); this relatively fine granularity gives an energy resolution of $\sigma/E = 24\%/\sqrt{E[\mathrm{GeV}]}$ for electromagnetic showers. The fibres collecting light from the scintillator are read out by photomultipliers and are grouped into sixteen calorimeter readout layers, perpendicular to the incident muons. The lengths of different layers vary from 13 to 18 radiation lengths of iron (X_0).

Particles of the momentum-analysed positive muon beam, with $E_\mu = 180$ GeV, were detected by three scintillator hodoscopes; the direction of incidence was measured by a pair of two-coordinate wire chambers.

Approximately 400 000 muon triggers were used in this analysis. A minimum-ionizing particle signal was required in the scintillator hodoscopes in order to suppress multi-particle events. Only events within a spot of 1.5x1.5 cm^2 in the beam chambers were used. In order to eliminate the very small hadron and electron contamination in the muon beam, only events that passed through the first five calorimeter layers (6 nuclear interaction lengths, or 64 radiation lengths) without producing showers were selected for analysis.

To be accepted, showers were required to have their maximum between the 6th and the 13th cell. This defined a fiducial region for observing showers of 115.3 radiation lengths. The expected number of remaining hadron–induced interactions in the fiducial region is less than 2 events. This was estimated by extrapolating the observed distribution of hadronic showers with maxima in the first three calorimeter layers. The number of muon decays in flight within the fiducial region was estimated to be 1.5 events, which is consistent with two events (see Fig. 3) with no muons downstream of the shower that were observed and excluded from the analysis.

The signal energy scale, *i.e.* the conversion factor used to obtain the energy of the showers from the digitized photomultiplier signals, was measured for the first layer using an electron beam. It was calculated for all other layers by equalizing for each layer the values of the Landau peak. This was obtained by fitting the muon signals with the convolution of Landau and Gaussian distributions [16]. The muon signal peak in each layer is determined with an error of about 1%. The intercalibration was crosschecked with calibration data obtained with a Cs^{137} gamma source

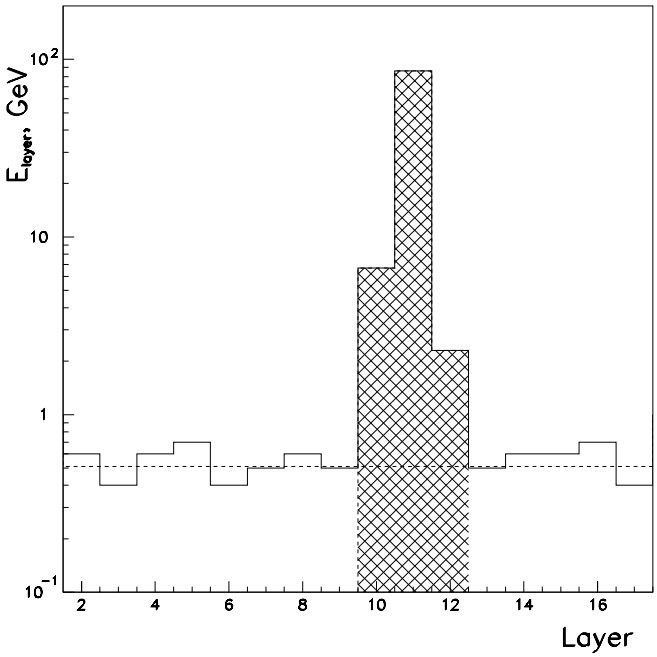

Fig. 4. An example of a 100 GeV electromagnetic shower as seen in the data. The energy $E_{\rm shower}$ is the sum of energies in three consecutive layers (hatched) corrected for underlying track ionization and overlapping showers (see text)

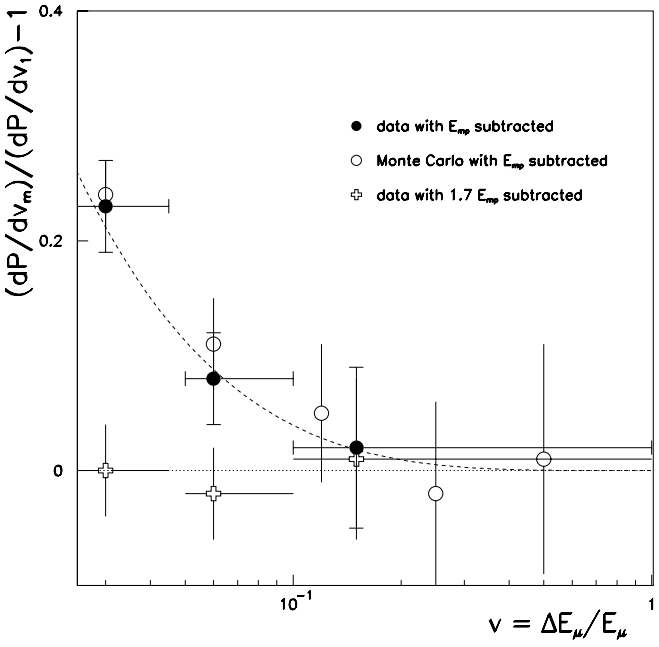

Fig. 5. The multiple shower contribution to the differential probability distribution $\mathrm{d}P/\mathrm{d}v$. Variables $\mathrm{d}P/\mathrm{d}v_{\rm m}$ and $\mathrm{d}P/\mathrm{d}v_1$ denote the differential probability with and without the multiple showers contribution respectively. The full circles correspond to fractional losses defined as $v_{\rm m} = (\Delta E_\mu - E_{\rm mp})/E_\mu$, the empty circles are Monte Carlo predictions. The crosses correspond to fractional energy losses defined as $v_{\rm m} = (\Delta E_\mu - 1.7 \cdot E_{\rm mp})/E_\mu$. The dashed curve is the approximation used to correct the data

[15] which also have an error of about 1%. The two independent calibrations correlate with an $r.m.s.$ of 1.5%.

The quantity to be compared to theoretical estimates is the differential probability $\mathrm{d}P/\mathrm{d}v$ of fractional muon energy loss v per radiation length. The fractional energy loss v is expressed as $v = \Delta E_\mu/(E_\mu - \epsilon)$, where the muon energy E_μ is corrected by the energy losses ϵ in layers preceding the shower signal. ΔE_μ is the shower energy, which is calculated excluding the underlying contribution from the minimum–ionizing track. To obtain ΔE_μ the signals in three consecutive layers centered on the maximal signal are summed and then corrected by subtracting the contributions from the muon track ionization and low energy showers overlapping in the three signal cells.

Two different methods have been used to perform the shower energy correction. In the first method, the most probable muon energy loss in the three signal cells is subtracted and then the overlapping shower correction is made. The latter correction is obtained by extrapolating the measured differential probability to zero layer thickness. The energy of the shower was evaluated as the sum of 3, 4 and 5 layers respectively; then $\mathrm{d}P/\mathrm{d}v$ was calculated for each of these cases and extrapolated to the case of zero layers. Thus measured, the contribution of multiple shower events to the differential probability $\mathrm{d}P/\mathrm{d}v$ is +23%, +10%, and +2% for v equal to 0.025, 0.06, and 0.15 respectively. These values agree well with the results of GEANT 3.21 simulations as shown in Fig. 5. The curve shown on Fig. 5 has been used to correct the values of $\mathrm{d}P/\mathrm{d}v$.

In the figure, one may also see that the subtraction of the mean muon signal truncated at 1.7 times the most probable value fully eliminates the overlapping showers contributions. This is the second method to perform the shower energy correction.

The differential energy loss probabilities were calculated with the two methods and averaged. The largest differences 3% are in the low v region. We take ±1.5% as an estimate of the uncertainty of the overlapping shower correction.

Finally the differential probability per radiation length of the fractional energy loss in the i-th interval of v was calculated as:

$$\frac{\mathrm{d}P}{\mathrm{d}v}(\langle v\rangle) \simeq \frac{\Delta P}{\Delta v} = \frac{(N_i/N_{\rm tot})}{\Delta v_i} \cdot \frac{1}{115.3} \frac{1 - cor_2(v)}{cor_1(v)},$$

where N_i is the number of events in the i-th interval, $N_{\rm tot}$ is the total number of analyzed events, Δv_i is the width of the i-th interval and $\langle v\rangle$ is the mean value of v within the interval.

The correction factor $cor_1(v)$ accounts for the loss of events of fractional energy v when an other shower of energy greater than v occurs in the fiducial region. The event is then counted with the higher of the two v values (as a consequence of searching for the peak energy deposition) and the ensuing loss at lower v must be corrected. The factor $cor_1(v)$ was calculated as $cor_1(v) = 1 - 115.3 X_0 \int_v^1 (dP/dv) dv$ using the theoretical value of $\mathrm{d}P/\mathrm{d}v$. The correction was checked by obtaining the $\mathrm{d}P/$

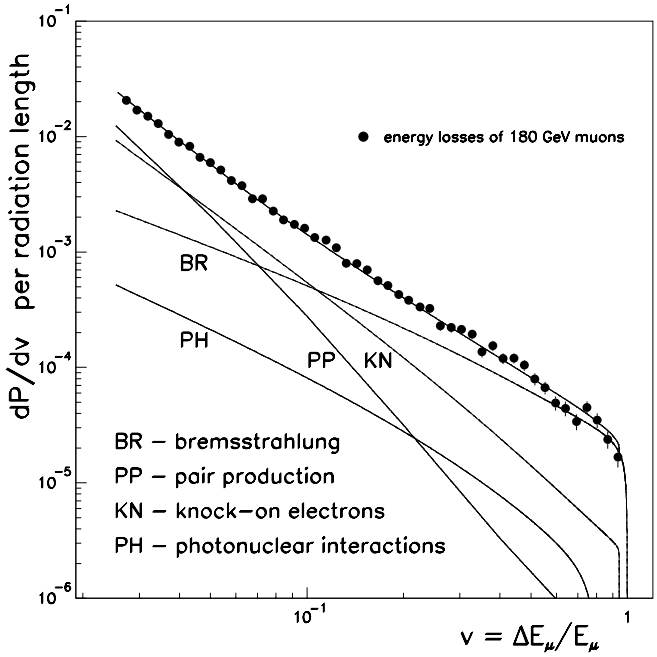

Fig. 6. The distribution of differential probabilities $\mathrm{d}P/\mathrm{d}v$ for the energy loss of 180 GeV muons in iron. The data (full circles) are compared to the sum of theoretical predictions for contributing processes described in the text: pair production (PP), knock-on electrons (KN), bremsstrahlung (BR) and photonuclear interactions (PH)

$\mathrm{d}v$ spectra over smaller fiducial regions (about 1/2 and 1/4 of the full analysis region) and comparing to the spectrum in the full region. The correction factor *vs.* v is thus obtained experimentally, and is found to be in agreement with the values calculated from theory. This correction for non-overlapping showers is important for the low end of the analyzed spectrum (0.94 for v=0.025) and is close to 1 for v >0.1.

The correction $cor_2(v)$ is applied to subtract from the data the showers that start in the scintillators (and other light materials) in order to compare the experimental results to the theoretical energy losses in iron. It varies from 1% to 3% over the range of v.

The lower limit of the analyzed energy loss spectrum was set to 4.5 GeV, because for this value the signal from the processes studied in this paper is sufficiently well separated from the most probable muon signal in three consecutive layers, which is about 1.2 GeV. The requirement to observe a muon downstream of the shower (in order to eliminate the background from muon decays) limited the upper edge of the analyzed spectrum to v=0.97.

The measured differential probabilities per radiation length of iron are given in Table 1 and are plotted in Fig. 6. The errors quoted are statistical only.

The systematic errors of the energy loss spectrum are dominated by the uncertainty on the signal energy scale (±1%) and by the estimated uncertainty on the muon energy (±1%). The contribution of these uncertainties to the systematic error on $\mathrm{d}P/\mathrm{d}v$ varies with energy. It is ±3.4% at v=0.025 and ±1.6% for v close to 1. The steel absorber composition is 99.5% iron, 0.4% manganese (with atomic number very close to iron) and less than 0.1% carbon. The uncertainty of the total absorber thickness is estimated to be ±0.3% and contributes by the same amount to the systematic error of $\mathrm{d}P/\mathrm{d}v$. The uncertainty of the overlapping showers correction contributes by ±1.5% to $\mathrm{d}P/\mathrm{d}v$ at low values of v. Altogether, the systematic error on the differential probability of the fractional energy loss $\mathrm{d}P/\mathrm{d}v$ varies from ±3.9% at v=0.025 to ±1.9% at the highest values of v.

3 Theoretical predictions

The theoretical predictions to be compared with these results are discussed next. Four different mechanisms contributing to the energy loss process have been considered.

Pair production: The Kelner and Kotov expression [17] for the differential probability per radiation length of muon energy loss by pair production is

$$\left(\frac{\mathrm{d}P}{\mathrm{d}v}\right)_{\mathrm{pair}} = C\frac{16}{\pi}Z(Z+\xi)\alpha^2\frac{1}{v}F(E_\mu, v)\ .$$

The constant C is given by $C = X_0\rho N_\mathrm{A} r_\mathrm{e}^2/A = 1.185 \cdot 10^{-2}$.

Here N_A is the Avogadro constant, r_e is the classical electron radius and α is the fine structure constant; X_0, ρ, A and Z are the radiation length, the density, the atomic weight, and the atomic number of iron respectively. The values of all constants are taken from [18]. The Kelner and Kotov function $F(E_\mu, v)$ for 180 GeV muon losses in iron is obtained from an interpolation of the tabulated values for lead and sodium at different energies [17]. The parameter ξ=0.95 takes into account pair production on atomic electrons [19].

Knock-on electrons. In order to describe the production of energetic knock-on electrons, the Bhabha formula [20] given by Rossi [21] is used (m_e is the electron mass and C is defined as above):

$$\left(\frac{\mathrm{d}P}{\mathrm{d}v}\right)_{\mathrm{knock-on}} = C2\pi Z\left(\frac{m_\mathrm{e}}{E_\mu}\right)\frac{1-\frac{v}{v_{max}}+\frac{v^2}{2}}{v^2} \cdot (1+\delta_{rad})\ ,$$

where $v_{max} = 1/(1 + m_\mu^2/2m_eE_\mu)$ is the maximal energy loss of a muon colliding with an electron (m_μ is the muon mass). Here, v_{max} =0.94; this kinematic limit produces visible kinks in the curves in Figs. 1 and 7. The correction δ_{rad} is the combined contribution of the so–called e-diagrams (photons emitted by the atomic electron) and α^3 - radiative corrections to the knock-on electron production [4]. The value of the correction varies slowly from 4% at v=0.025 to about 8% for v close to v_{max}. The result of this correction is an almost constant increase of the differential probability of total muon energy losses (the sum of all described processes) by about 2% over the whole v range.

Table 1. The measured differential probability values $\Delta P/\Delta v$ per radiation length for fractional energy losses v of 180 GeV muons in iron. The errors quoted are statistical

$\langle v \rangle$	$\Delta P/\Delta v$	$\langle v \rangle$	$\Delta P/\Delta v$
$(2.736 \pm 0.002) \times 10^{-2}$	$(2.06 \pm 0.06) \times 10^{-2}$	$(1.666 \pm 0.003) \times 10^{-1}$	$(5.6 \pm 0.4) \times 10^{-4}$
$(2.949 \pm 0.002) \times 10^{-2}$	$(1.69 \pm 0.05) \times 10^{-2}$	$(1.790 \pm 0.003) \times 10^{-1}$	$(5.1 \pm 0.4) \times 10^{-4}$
$(3.185 \pm 0.002) \times 10^{-2}$	$(1.50 \pm 0.05) \times 10^{-2}$	$(1.930 \pm 0.003) \times 10^{-1}$	$(4.3 \pm 0.4) \times 10^{-4}$
$(3.435 \pm 0.003) \times 10^{-2}$	$(1.30 \pm 0.04) \times 10^{-2}$	$(2.076 \pm 0.003) \times 10^{-1}$	$(3.8 \pm 0.3) \times 10^{-4}$
$(3.701 \pm 0.003) \times 10^{-2}$	$(1.04 \pm 0.04) \times 10^{-2}$	$(2.250 \pm 0.004) \times 10^{-1}$	$(3.3 \pm 0.3) \times 10^{-4}$
$(3.990 \pm 0.003) \times 10^{-2}$	$(9.0 \pm 0.3) \times 10^{-3}$	$(2.415 \pm 0.004) \times 10^{-1}$	$(3.2 \pm 0.3) \times 10^{-4}$
$(4.310 \pm 0.004) \times 10^{-2}$	$(8.3 \pm 0.3) \times 10^{-3}$	$(2.609 \pm 0.005) \times 10^{-1}$	$(2.3 \pm 0.2) \times 10^{-4}$
$(4.636 \pm 0.004) \times 10^{-2}$	$(6.6 \pm 0.3) \times 10^{-3}$	$(2.818 \pm 0.006) \times 10^{-1}$	$(2.2 \pm 0.2) \times 10^{-4}$
$(5.002 \pm 0.004) \times 10^{-2}$	$(5.9 \pm 0.3) \times 10^{-3}$	$(3.033 \pm 0.006) \times 10^{-1}$	$(2.1 \pm 0.2) \times 10^{-4}$
$(5.388 \pm 0.005) \times 10^{-2}$	$(5.1 \pm 0.2) \times 10^{-3}$	$(3.273 \pm 0.006) \times 10^{-1}$	$(1.9 \pm 0.2) \times 10^{-4}$
$(5.811 \pm 0.006) \times 10^{-2}$	$(4.2 \pm 0.2) \times 10^{-3}$	$(3.520 \pm 0.008) \times 10^{-1}$	$(1.4 \pm 0.2) \times 10^{-4}$
$(6.267 \pm 0.007) \times 10^{-2}$	$(3.8 \pm 0.2) \times 10^{-3}$	$(3.803 \pm 0.008) \times 10^{-1}$	$(1.5 \pm 0.2) \times 10^{-4}$
$(6.756 \pm 0.007) \times 10^{-2}$	$(2.9 \pm 0.2) \times 10^{-3}$	$(4.093 \pm 0.009) \times 10^{-1}$	$(1.2 \pm 0.1) \times 10^{-4}$
$(7.276 \pm 0.008) \times 10^{-2}$	$(2.9 \pm 0.2) \times 10^{-3}$	$(4.42 \pm 0.01) \times 10^{-1}$	$(1.2 \pm 0.1) \times 10^{-4}$
$(7.848 \pm 0.009) \times 10^{-2}$	$(2.3 \pm 0.1) \times 10^{-3}$	$(4.77 \pm 0.01) \times 10^{-1}$	$(1.1 \pm 0.1) \times 10^{-4}$
$(8.46 \pm 0.01) \times 10^{-2}$	$(1.9 \pm 0.1) \times 10^{-3}$	$(5.14 \pm 0.01) \times 10^{-1}$	$(7.9 \pm 0.9) \times 10^{-5}$
$(9.13 \pm 0.01) \times 10^{-2}$	$(1.7 \pm 0.1) \times 10^{-3}$	$(5.53 \pm 0.02) \times 10^{-1}$	$(6.7 \pm 0.8) \times 10^{-5}$
$(9.83 \pm 0.01) \times 10^{-2}$	$(1.61 \pm 0.09) \times 10^{-3}$	$(5.97 \pm 0.02) \times 10^{-1}$	$(4.9 \pm 0.7) \times 10^{-5}$
$(1.057 \pm 0.001) \times 10^{-1}$	$(1.34 \pm 0.08) \times 10^{-3}$	$(6.40 \pm 0.02) \times 10^{-1}$	$(4.4 \pm 0.6) \times 10^{-5}$
$(1.147 \pm 0.002) \times 10^{-1}$	$(1.27 \pm 0.08) \times 10^{-3}$	$(6.93 \pm 0.02) \times 10^{-1}$	$(3.4 \pm 0.5) \times 10^{-5}$
$(1.234 \pm 0.002) \times 10^{-1}$	$(1.09 \pm 0.07) \times 10^{-3}$	$(7.48 \pm 0.02) \times 10^{-1}$	$(4.5 \pm 0.6) \times 10^{-5}$
$(1.327 \pm 0.002) \times 10^{-1}$	$(8.0 \pm 0.6) \times 10^{-4}$	$(8.05 \pm 0.02) \times 10^{-1}$	$(3.5 \pm 0.5) \times 10^{-5}$
$(1.431 \pm 0.002) \times 10^{-1}$	$(7.9 \pm 0.6) \times 10^{-4}$	$(8.66 \pm 0.03) \times 10^{-1}$	$(2.4 \pm 0.4) \times 10^{-5}$
$(1.541 \pm 0.002) \times 10^{-1}$	$(7.0 \pm 0.5) \times 10^{-4}$	$(9.33 \pm 0.03) \times 10^{-1}$	$(1.7 \pm 0.3) \times 10^{-5}$

Bremsstrahlung. The expression for bremsstrahlung is usually written as:

$$\left(\frac{\mathrm{d}P}{\mathrm{d}v}\right)_{\text{bremsstrahlung}} = C4Z^2\alpha\left(\frac{m_\mathrm{e}}{m_\mu}\right)^2\frac{1}{v} \times\left(\frac{4}{3}-\frac{4}{3}v+v^2\right)\Phi(\delta(v)),$$

where the screening function Φ depends on the minimum momentum transfer to the nucleus $\delta = m_\mu^2 v/2E_\mu(1-v)$.

The screening function consists of several terms:

$$\Phi(\delta) = \Phi_0(\delta) - f_{coul} - \Delta_a^{el}(\delta) - \Delta_n^{el}(\delta) + \frac{f_a^{inel}(\delta)}{Z} + \frac{f_n^{inel}(\delta)}{Z}.$$

The main term $\Phi_0(\delta)$ corresponds to muon bremsstrahlung on the Coulomb center in the Born approximation. The value of Φ_0 is 9, 5.5 and 0 for v equal to 0.2, 0.9 and 1 respectively. The term $\Phi_0(\delta)$ is known to better than 1%.

The value of the correction factor f_{coul} for iron is 0.042. It is given in [22] for electron bremsstrahlung, and in [5] for muons.

Δ_a^{el} is the correction for screening of the nucleus by atomic electrons. Δ_a^{el} is known to about $\pm 2\%$. This correction varies from 0.5 for $v = 0.2$ to 0 for $v \to 1$.

The effect of the nuclear form factor is described in [4]

$$\Delta_n^{el}(\delta) = ln\left(\frac{e^{\Delta_n^{el}}}{1+\delta(e^{\Delta_n^{el}}\sqrt{e}-2)/m_\mu}\right) \simeq \Delta_n^{el}$$

and is approximated by a constant Δ_n^{el}. Values of Δ_{Fe}^{el} between 0.5 and 1.5 are predicted by different theoretical calculations. All these corrections decrease the cross section.

The last two corrections account for inelastic processes with atomic electrons and the nucleus. The corrections are positive; however, they are suppressed by a factor 1/Z. The atomic inelastic correction describes the contribution of the so–called μ-diagrams (the photon is emitted by the incident muon in a muon-electron interaction). For the correction to the integrated losses, this is usually taken into account by replacing the Z^2 term in the cross section formula by the term $Z(Z+\xi)$ with ξ close to 1. For the differential spectrum given here, the expression [4]:

$$\frac{f_a^{inel}(\delta)}{Z} = \frac{1}{Z}\left(ln\frac{m_\mu/\delta}{\delta m_\mu/m_e^2+\sqrt{e}} - ln\left(1+\frac{1}{\delta\sqrt{e}B'Z^{-2/3}/m_e}\right)\right)$$

is used.

The value of the correction is about 0.3 for v =0.2 and is close to 0 for $v \to 1$. The value of the correction is known

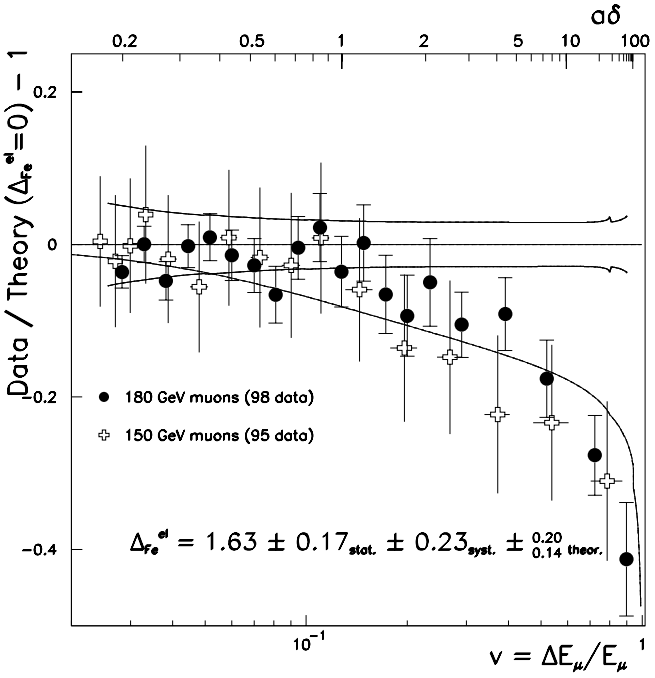

Fig. 7. Determination of Δ_{Fe}^{el}, the elastic nuclear form factor correction to muon bremsstrahlung. The data (full circles) are compared with theoretical predictions with $\Delta_{Fe}^{el} = 0$ (horizontal line at 0) and the fit to the data with Δ_{Fe}^{el}=1.63 shown by the curve. The effect of systematic errors is shown by the two curves around zero. For comparison, the data of [14] are plotted by crosses. The error bars are the quadratic sum of statistical and systematic errors. The upper horizontal scale is in units of the product of the Bohr radius of the iron atom (a) and the minimal momentum transfer to the iron nucleus (δ). The values of $a\delta$ determine the regions of screening ($a\delta \leq 1$) and of no screening ($a\delta \geq 1$) of the nucleus by atomic electrons

to better than ±0.5%. The nuclear inelastic correction is expressed as a function of the nuclear elastic correction:

$$\frac{f_n^{inel}(\delta)}{Z} = \frac{\Delta_n^{el}(\delta)}{Z}.$$

Photonuclear interactions: Photonuclear interactions also contribute to the muon energy loss. The probability calculated by Bezrukov and Bugaev [23] is given in [24] (see the detailed description of different terms there):

$$\left(\frac{\mathrm{d}P}{\mathrm{d}v}\right)_{\text{photonuclear}} = C\left(\frac{A\sigma_{\gamma N}(\epsilon)}{\pi r_{\mathrm{e}}^2}\right)\frac{\alpha}{2}v\Gamma(E_\mu, v),$$

The contribution of photonuclear interactions is about 1% for the lowest value of the measured fractional loss v and about 5% for the highest v value. The energy loss, however, is underestimated by summing the energy deposition in only three layers of Module 0 and also because the response of the calorimeter to hadrons is lower than that for electrons (e/h=1.34 [15]). Using pion beam data it was estimated that about 75% of the energy of photonuclear hadronic showers is contained in three consecutive layers.

Table 2. The sources of systematic errors of Δ_{Fe}^{el}

Source	variation of Δ_{Fe}^{el}
acceptance	±0.07
energy scale	±0.20
multiple showers	±0.10
combined experimental	±0.23
pair production	±0.06
knock-on electrons	±0.05
bremsstrahlung	±0.08
diffractive correction	+0.14
photonuclear	±0.09
combined theoretical	$\pm^{0.20}_{0.14}$

Altogether, the contribution to $\mathrm{d}P/\mathrm{d}v$ of photonuclear interactions was about 2.5% in the region of highest energy losses.

4 Comparison of experiment and theory

It Fig. 6 the experimental energy loss spectrum is compared to the sum of the four contributions described above.

The experimentally obtained differential probabilities of muon fractional energy loss per radiation length of iron are given in Table 1 and plotted in Fig. 6. The theoretical values, which are the sum of the predictions for the four processes described above, are in very good agreement with the experimental results over the range of fractional energy losses v from 0.025 to 0.12. This is the region of screening of the nucleus by the electron cloud, where the Bohr radius of iron in the Thomas-Fermi model, $a = 2.19{\cdot}10^5$ GeV^{-1}, and the minimum momentum transfer to the nucleus δ, defined above, fullfill the relation: $1/\delta \geq a$. In this region only larger momentum transfers, corresponding to radii inside the electron cloud, effectively contribute to bremsstrahlung, while the electron cloud screens the processes with smaller momentum transfer.

The region $v \geq 0.12$ is the region of no screening. In this region the dominant process for muon energy losses is bremsstrahlung (see Fig 6). With these new and more precise data it is possible to measure the value of Δ_{Fe}^{el} in this region. The nuclear elastic form factor correction Δ_{Fe}^{el} is not known experimentally, and there are several theoretical predictions, which vary from 0.5 to 1.5 [9,28, 27,26,25,4,5,29]. The value of $\Delta_{Fe}^{el} = 1.5$ corresponds to approximately a 15% reduction of the total muon energy losses at v=0.75 compared to the losses for $\Delta_{Fe}^{el} = 0.5$.

Theories also differ in the prediction of the nuclear size correction to muon bremsstrahlung in the region of screening. It is predicted to be negligible in [30], while the value of about 1.5 (the same as for the region of no screening) is predicted in [4,25,5,29]. The results of this experiment are insensitive to its value in the region of screening (low values of v), because in this region the bremsstrahlung

Table 3. The comparison of the theoretical predictions and the measured value of the iron nuclear elastic form factor correction Δ^{el}_{Fe}. The value of $\sigma_{\Delta^{el}_{Fe}}$ used is the quadratic sum of statistical, systematic and theoretical errors

Reference	$\Delta^{el}_{Fe}(theory)$	$\frac{\Delta^{el}_{Fe}(theory)-\Delta^{el}_{Fe}(meas)}{\sigma_{\Delta^{el}_{Fe}}}$
[9,28]	0.52	-3.5
[27]	0.68	-3.0
[26]	0.90	-2.3
[4,25]	1.52, 1.49	-0.3
[5,29]	1.44	-0.6
This measurement:	$1.63 \pm 0.17_{stat} \pm 0.23_{syst} \pm^{0.20}_{0.14 theor}$	

process contributes only a small part of the total energy loss probability.

The data have been compared with theoretical predictions using the value of $\Delta^{el}_{Fe} = 0$ (see Fig. 7). The deviation from a flat distribution is an indication of a non zero value of Δ^{el}_{Fe}. Its value has been measured by fitting the data to the theoretical predictions with Δ^{el}_{Fe} as a free parameter. The result is shown in Fig. 7.

The combined effect of systematic errors due to uncertainties in the acceptance, energy scale and multiple shower corrections is shown in Fig. 7 by two lines around the zero.

The errors of the theoretical predictions must also be considered. We estimate that the pair production process spectrum has an error of ±3%, mainly due to the interpolation of the tabulated function $F(E_\mu, v)$.

The main possible source of theoretical uncertainties in Δ^{el}_{Fe} is the description of the electron knock-on process, because it gives the second–largest contribution to energy losses (after bremsstrahlung) in the high energy region. The radiative correction to knock-on electron process δ_{rad} was assigned a conservative error of 30%.

For the bremsstrahlung process, an error was estimated for each of the individual terms of the screening functions given above. As shown in [6], for positively charged muons bremsstrahlung should be corrected for diffraction of a hard photon on a nucleus. The correction increases the bremsstrahlung cross section of 180 GeV muons in rock by about 4%. The correction of 2.5% for iron has been estimated using the A and Z dependence of the diffractive cross section.

An error of ±30% for the contribution of the photonuclear interactions has been assumed. All systematic errors are summarized in Table 2.

Finally, the result for the nuclear elastic form factor correction to muon bremsstrahlung in iron is:

$$\Delta^{el}_{Fe} = 1.63 \pm 0.17_{stat} \pm 0.23_{syst} \pm^{0.20}_{0.14 theor}.$$

5 Summary and conclusions

The results on muon energy losses in iron reported in this paper are statistically in agreement with those previously published by the same authors [14]. They confirm that the description of the entire muon energy loss spectrum by a combination of electromagnetic processes is entirely adequate. However the new results are a significant improvement on the previous ones [14] because of the much larger size of the detector, which in turn allowed a more precise and sophisticated analysis and smaller systematics. Specifically, the readout segmentation in the muon direction made it possible to cross–check with the data the procedure to eliminate the signal from overlapping showers, as well as the correction for non-overlapping showers in the fiducial region. Also, in this paper the energy scale of the muon–induced showers is determined and cross–checked with independent calibration data, thereby greatly reducing the contributions to the error on the energy loss spectrum from this source.

The sensitivity achieved for higher fractional energy losses allowed to measure for the first time the effect on muon bremsstrahlung of the nuclear elastic form factor. The theoretical predictions vary from no effect to a -30% effect at the upper end of the energy loss spectrum. The results are precise enough to discriminate between different theoretical calculations; specifically, they are in agreement with two sets of predictions ([4,25] and [5,29]), while they differ from three other sets by 2.3 to 3.5 standard deviations (see Table 3).

The experimental results obtained in this paper support the calculations of muon stopping power and range given in the tables of [31], which are based on the same formulae for electron–positron pair production and bremsstrahlung as this paper, and on the value of the nuclear elastic form factor given in [4].

Acknowledgements. We sincerely thank the technical staffs of the collaborating Institutes for their important and timely contributions. Financial support is acknowledged from the funding agencies of the collaborating Institutes. Finally, we are grateful to the staff of the SPS, and in particular to K. Elsener, for the excellent beam conditions and assistance provided during our tests.

References

1. ATLAS Collaboration, ATLAS Technical Proposal, report CERN/LHCC/94–43
2. S.R. Kelner, R.P. Kokoulin, A.A. Petrukhin, Phys. Atom. Nucl. **60**, (1997) 657
3. M.J. Tannenbaum, preprint CERN-PPE/91-134 (1991)
4. S.R. Kelner, R.P. Kokoulin, A.A. Petrukhin, preprint 024-95, Moscow Technical University, 1995
5. Yu.M. Andreev, E.V. Bugaev, Phys. Rev. **D55**, (1997) 1233
6. S.R. Kelner, A.M. Fedotov, Phys. Atom. Nucl. **62**, (1999) 307
7. W. Stamm et al., Nuovo Cim. **51A**, (1979) 242
8. K. Mitsui et al., Nuovo Cim. **73A**, (1983) 235
9. W.K. Sakumoto et al., Phys.Rev. **D45**, (1992) 3042
10. J.J. Aubert et al., Z. Phys. **C10**, (1981)
11. R. Kopp et al., Z. Phys. **C28**, (1985) 171
12. R. Baumgart et al., Nucl. Instrum. Methods **A258**, (1987) 51
13. M. Antonelli, G. Battistoni, A. Ferrari, P.R. Sala, Proceedings of the 6th International Conference on Calorimetry in High–energy physics, 1996, Frascati, Italy, p. 561. see also ATLAS Collaboration, Calorimeter Performance Technical Design Report, CERN/LHCC 96-40, CERN, 1997, p. 150–152
14. E. Berger et al., Z. Phys. **C73**, (1997) 455–463; CERN-PPE/96-115, CERN 1996
15. F. Ariztizabal et al., Nucl. Instrum. Methods **A349**, (1994) 384. E. Berger et al., report CERN/LHCC 95–44. Atlas Collaboration, Tile Calorimeter TDR, CERN/LHCC 96-42
16. T. Davidek, R. Leitner, ATLAS Internal Note ATL-TILECAL-97-114 (1997)
17. S.R. Kelner, Yu.D. Kotov, Sov. J. Nucl. Phys. **7**, (1968) 360
18. Particle Data Group, Eur. Phys. J. **C3**, (1998) 1
19. S.R. Kelner, Phys. Atom. Nucl. **61**, (1998) 448
20. H.J. Bhabha, Proc. Roy. Soc. **A164**, (1938) 257
21. B. Rossi, High Enery Particles, Prentice-Hall, New York, 1952
22. H. Davies, H.A. Bethe, L.C. Maximon, Phys. Rev. **93**, (1954) 788
23. L.B. Bezrukov, E.V. Bugaev, Sov. J. Nucl. Phys. **33**, (1981) 635
24. W. Lohmann et al., CERN report 85–03 (1985)
25. A.A. Petrukhin, V.V. Shestakov, Can. J. Phys. **46**, (1968) S377. R.P. Kokoulin, A.A. Petrukhin, Acta Phys. Acad. Sci. Hung. 29 Suppl. **4**, (1970) 277
26. R.F. Christy, S. Kusaka, Phys. Rev. **59**, (1941) 405
27. I.L. Rozentahl, Usp. Fiz. Nauk **94**, (1968) 91
28. A.D. Erlykin, Proc. 9th ICCR, London, 2 (1966) 999
29. Yu.M. Andreev, L.B. Bezrukov, E.V. Bugaev, Phys. Atom. Nucl. **57**, (1994) 2066
30. Y. Tsai, Rev. Mod. Phys. **46**, (1974) 815
31. D.E. Groom, N.V. Mokhov, S.I. Striganov, LBNL-44742, submitted to Atomic Data and Nuclear Data Tables